Switches to rhythmic brain activity lead to a plasticity-induced reset in synaptic weights

Kathleen Jacquerie, Caroline Minne, Juliette Ponnet, Nora Benghalem, Pierre Sacré, and Guillaume Drion

Department of Electrical Engineering and Computer Science, University of Liege, Belgium

Keywords: *synaptic plasticity*, *STDP*, *calcium-dependent plasticity*, *brain states*, *excitability neuromodulation*, *homeostasis*

Abstract

Brain function relies on the ability to quickly process incoming information while being capable of forming memories of past relevant events through the formation of novel synaptic connections. Synaptic connections are functionally strengthened or weakened to form new memories through synaptic plasticity rules that strongly rely on neuronal rhythmic activities. Brain information processing, on the other hand, is shaped by fluctuations in these neuronal rhythmic activities, each defining distinctive brain states, which poses the question of how such fluctuations in brain states affect the outcome of memory formation. This question is particularly relevant in the context of sleep-dependent memory consolidation, wakefulness to sleep transitions being characterized by large modifications in global neuronal activity. By combining computational models of neuronal activity switches and plasticity rules, we show that switches to rhythmic brain activity reminiscent of sleep lead to a reset in synaptic weights towards a basal value. This reset is shown to occur both in phenomenological and biophysical models of synaptic plasticity, and to be robust to neuronal and synaptic variability and network heterogeneity. Analytical analyses further show that the mechanisms of the synaptic reset are rooted in the endogenous nature of the sleep-like rhythmic activity. This sleep-dependent reset in synaptic weights permits regularizing synaptic connections during sleep, which could be a key component of sleep homeostasis and has the potential to play a central role in sleep-dependent memory consolidation.

Introduction

Our brain has the ability to process information to quickly analyze or react to incoming events from the environment, as well as to learn from experience to shape our memory. This information processing is built on fluctuations in rhythmic neuronal patterns at the cellular and population levels, each *defining brain states* [1–3]. These patterns are spatiotemporal signatures of large neuronal populations. The switches between different brain states can be fast and localized, as observed for instance in brain areas prior to movement initiation [4], or global and long-lasting, such as those characterizing wake-sleep cycles [1, 5, 6]. These rhythms translate the collective activity of neurons interconnected via synaptic connections.

At the cellular level, neurons are able to switch between different modes of excitability under the control of *neuromodulators* [7]. In particular, the transition from wakefulness to sleep is associated with dramatic modifications in neuromodulator concentrations, such as serotonin, norepinephrine, dopamine and acetylcholine, which in turn induces a switch in neuronal activity in many brain regions from asynchronous spiking to a rhythmic bursting activity [8]. These fluctuations have been shown to critically shape memory, a property that is called sleep-dependent memory consolidation [9–11].

On the other hand, memory relies on the ability of neurons to modify their connections with other cells through a mechanism called synaptic plasticity [12, 13]. A great deal of attention has been paid to understand the rules of synaptic plasticity in behavior and learning [14]. Two categories of synaptic plasticity models are common in the literature. The first one considers simple spike time series as inputs for the plasticity rule, [15, 16] and the second uses calcium as a key driver [17, 18]. The validity and the role of these synaptic plasticity rules in shaping how a neuronal network learns specific tasks has been extensively studied. However, our understanding of how such rules interact with the fluctuations in brain states we observe during the sleep-wake cycle is still scarce [19–21].

In this paper, we explore how networks switch from asynchronous spiking to rhythmic bursting as those observed in the wake-sleep transition affect the outcome of several synaptic plasticity rules. We construct a neuronal circuit capable of reproducing the transition from tonic firing to bursting under the control of neuromodulators. This circuit is made of conductance-based models and comprises inhibitory neurons projecting GABA currents onto two layers of excitatory neurons connected through AMPA currents. The synaptic connection between the two excitatory neuron layers is governed by a synaptic plasticity rule. We compare 20 different rule variations, ranging from spike-time dependent plasticity rules (such as pair-based and triplet [15, 16, 22–24]) to calcium-dependent rules [17, 25, 26]. All rules are parameterized in the spiking regime to fit experimental data obtained either on a spike-timing protocol [27] or on a frequency-pairing protocol [28]. We then compare how strong and weak synaptic weights acquired during wakefulness evolve as the network switches in rhythmic bursting mode, an endogenous firing activity associated to sleep.

A switch to a rhythmic activity results in a reset of synaptic weights: whatever the strength established during wakefulness, the network resets its connectivity to a single steady-state value during sleep, regardless of the implemented plasticity rule, either being spike-time dependent or calcium-based. We call this phenomenon a *homeostatic reset* of synaptic weights, as it fully relies on endogenous properties of the network and promotes the regularization of synaptic weights during sleep. The homeostatic reset is shown to be robust to the level of neuromodulation, and to both variability and heterogeneity in circuit parameters. Further analytical investigations show that the mechanisms underlying the reset are rooted in the interactions between the endogenous dynamics of network rhythmic activity and the plasticity rules themselves, both being largely independent from initial synaptic weights.

Results

Switches to a rhythmic brain state reminiscent of sleep lead to a homeostatic reset of synaptic weights

We first investigated how switches in brain states, neuromodulation of activity, and synaptic plasticity interact by implementing a Spike-Timing-Dependent Plasticity (STDP) rule from [15] in a neuron circuit capable of switching between asynchronous spiking and rhythmic bursting states [1, 29]. The neuron circuit follows a conductance-based modeling paradigm and reproduces the activities observed in cortical networks during switches brain states [3, 8, 30], among others. The circuit is composed of an inhibitory neuron projecting GABA currents onto two excitatory neurons connected by an AMPA current (Figure 1A, left). This 3-cell circuit provides an appropriate support to study the transition between several firing activities and its functional consequence on the evolution of synaptic weight. Indeed, this topology is often encountered in different brain regions; such as the thalamus between reticular and relay cells [31, 32], the cortex between pyramidal and inhibitory cells [33, 34], or even between different organs like striatum and basal ganglia [4, 35]. Applying a hyperpolarizing current to the inhibitory cell, which models the effect of neuromodulators in our example (labeled NMOD in Figure 1A), switches the whole circuit from asynchronous slow tonic firing to synchronous bursting, which mimics the type of switch observed during transitions from wakefulness to sleep (Figure 1A, right - more details on the circuit in *SI Appendix*).

We then integrated a synaptic plasticity rule between the two excitatory neurons in the circuit. The connection strength between the neurons, or synaptic weight, is characterized by a variable w (Figure 1A). Synaptic plasticity is modeled by a synaptic rule describing the evolution of the synaptic weight throughout time, which we call Δw for conciseness (Figure 1A, right). Classical STDP was used as the synaptic plasticity mechanism in the neuronal model due to its prevalence in the synaptic plasticity literature, using a triplet model [15]. Because such plasticity rule is often not used in combination with conductance-based models, it was parameterized in the spiking regime to fit well-established experimental data obtained through a frequency pairing protocol [28] (more details on the parameter model fitting see *SI Appendix*).

To investigate how switches in brain states affect synaptic connections in the presence of STDP, we subjected six circuit models to two transitions from wakefulness to sleep and back, while letting the plasticity rule run its course (Figure 1B, see Methodsfor details). Among these six circuits, three were designed to exhibit a correlated activity between the excitatory neurons with the presynaptic neuron firing slightly before the postsynaptic neuron, mimicking the activity of neurons receiving functionally related inputs (dark blue curves in Figure 1B). The three others were designed to exhibit an uncorrelated, random activity, mimicking the activity of neurons receiving unrelated inputs (light blue curves in Figure 1B). We then compared the evolution of the synaptic weight in these six circuits along the two wake-sleep cycles (see middle panel of Figure 1B).

During wakefulness, neurons are in spiking mode and the synaptic weights evolve in accordance with the level of correlation between the presynaptic and postsynaptic neurons, in agreement with the STDP rule. The connection strengths between neurons exhibiting correlated activities increase(Figure 1B, top left), whereas the connection strengths between neurons exhibiting uncorrelated activities decrease (Figure 1B, bottom left).

As the circuit switches to sleep, the neurons switch to a rhythmic bursting mode. This change in activity radically affects the time evolution of the synaptic weights under the STDP rule: connections that were potentiated during the previous wakefulness phase start to depress (Figure 1B, top right), whereas connections that were depressed start to potentiate (Figure 1B, bottom right), and all connection strengths eventually converge to a single, stable point. This convergence point is fully independent of what happened during wakefulness. We call this phenomenon a *homeostatic reset* of synaptic weights, as it relies on a switch to an endogenous, rhythmic activity of the network and his independent from external inputs and learning history.

The potential functional consequences of the homeostatic reset are twofold. On the one hand, it promotes the regularization of synaptic weights during sleep, which in turn restores the ability to learn

new information on the next day. On the other hand, it potentially disrupts any learning that may have occurred during the previous day, if one solely relies on the evolution of w under the STDP rule.

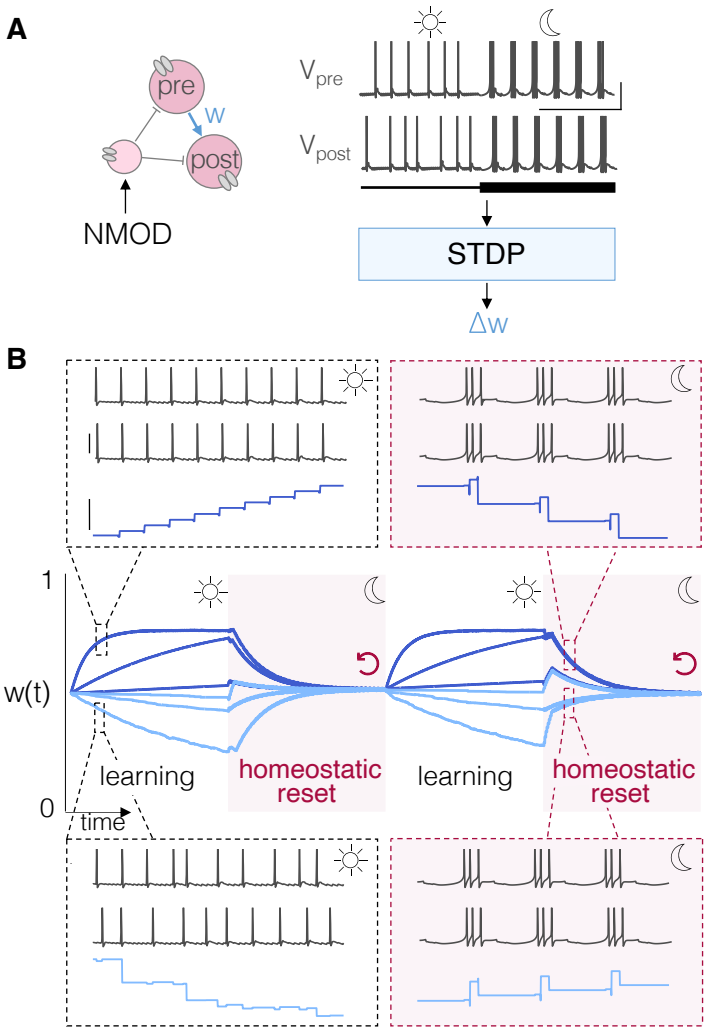

Figure 1: A homeostatic reset of synaptic weights is observed during rhythmic bursting mode whatever the neuronal activity correlation in tonic spiking
A. (Left) scheme of the three-cell circuit. The circuit is composed of an inhibitory cell (I) (depicted by the small light pink circle) that projects GABA current onto excitatory pre- and postsynaptic neurons. Applying neuromodulators (labeled by NMOD, black line) onto the I-cell induces the transition from tonic (☼) to burst (☾) in the circuit. The synaptic weight w between the excitatory neurons is affected by a spike time-dependent synaptic plasticity rule (STDP). (Right) Time evolution of membrane potentials of the circuit on tonic mode (modeling wakefulness), and rhythmic bursting mode (modeling sleep). (x-scale: 1 s, y-scale: 50 mV.)
B. Evolution of the synaptic weight in 6 circuits during two wake-sleep transitions. During wakefulness (☼), 3 circuits have a strong (resp. weak) correlated activity between pre- and post-synaptic neurons resulting in a synaptic weight increase (resp. decrease) shown in dark (resp. light) blue. During sleep mode (☾), all the synaptic weights are reset to the same value—a phenomenon that we called the *homeostatic reset*. Top and bottom panels provide zooms on the voltage traces and the associated synaptic weight evolution during spiking mode (learning) and bursting mode (homeostatic reset). (time window of 1 s, y-scale: 50 mV for V_m and 1 % for w.)

The homeostatic reset occurs in both phenomenological and biophysical models of synaptic plasticity

So far, we have seen that a classical STDP rule leads to a homeostatic reset in synaptic weights during a switch in network state from wakefulness to sleep. We further investigated the generality

of the homeostatic reset by testing 20 variations of 7 published synaptic plasticity models. These synaptic plasticity models can be split into two categories (Figure 2A). The first category comprises phenomenological models, which use spike timing of presynaptic and postsynaptic neurons as the main input that drives changes in synaptic weights. Prominent examples of such models are the pair-based rule using the pre- and post-spiking times [16, 23] and the triplet rule using pre-post-pre- or post-pre-post-spiking activity to change the synaptic weight [15, 25] (Figure 2A, left blue box). The second category comprises biophysical models, which use intracellular calcium concentration as the key signal that drives synaptic change [17, 18, 25, 26] (Figure 2A, right blue box). The two representations into the blue boxes are simplified to provide a comprehensive overview of the rules. Their computational implementations are described in *SI Appendix*. Then, we compare two different *weight-dependency plasticity* for each category of model by implementing either hard bounds or soft bounds (more information in [36, 37]).

Altogether, 2 phenomenological rules (see Table 1) and 5 calcium-dependent plasticity rules (see Table 2) are studied in this paper. Each parameter set is related to a region, a pairing protocol, a type of bounds and other factors listed in Tables 1 and 2.

Name	Region	Bounds	Reference	ID
Pair-based	H	Soft	[23]	1
	H	Hard	[16]	2
Triplet	H	Soft	adapted from [15]	3
	H	Hard	[15]	4
	C	Soft	[25]	5
	C	Hard	[15]	6

Table 1: Phenomenological models covered in this paper. Region is linked to the parameter choice depending on the brain area where the rule is fitted: (C) cortex, (H) hippocampus. The weight-dependency is either modeled by (Soft) soft bounds or (Hard) hard bounds.

Model	Formalism	Region	Bounds	Ca^{2+}-coupling	STD	Reference	ID
Graupner 2016	Th*	C	Soft	No	No	[25]	1
	Th	C	Soft	No	No	adapted from [25]	2
	Th	H	Soft	No	No	adapted from [25]	3
	Th	C	Hard	No	No	adapted from [25]	9
Graupner 2012	Th	C	Soft	No	No	[18]	4
	Th	H	Soft	No	No	[18]	5
Shouval 2002	Cont	C	Soft	No	No	adapted from [17]	6
	Cont	C	Hard	No	No	adapted from [17]	10
Deperrois 2020	Th	C	Soft	Yes	No	[26]	7
	Th	C	Hard	Yes	No	adapted from [26]	11
	Cont	C	Hard	Yes	No	adapted from [26]	12
Deperrois 2020	Th	C	Soft	Yes	Yes	[26]	8
	Th	C	Hard	Yes	Yes	adapted from [26]	13
	Cont	C	Hard	Yes	Yes	adapted from [26]	14

Table 2: Biophysical models investigated in this paper. (Th*) stands for calcium thresholds such as two opposing calcium-triggered pathways leading increases or decreases of synaptic strength [18, 25, 26]. (Th) uses calcium-dependent steady state value and time-constant. (Cont) stands for the continuous function of the calcium dependency [17]. Region is linked to the parameter choice depending on the brain area where the rule is fitted: (C) cortex, (H) hippocampus. The weight-dependency is either modeled by soft bounds (Soft) or hard bounds (Hard). (Ca^{2+}-coupling) The presynaptic calcium influx is coupled with the synaptic weight (Yes/No). The models include an equation considering the depression of presynaptic vesicles labeled short-term depression (STD) (Yes/No). The parameters come from an original paper or are adapted to reproduce the frequency dependency in a pairing protocol (for cortex as in [28]) or a STDP protocol (for hippocampus as in [27]).

This raised the issue that fitting plasticity rule is a complex problem. The paper aiming at comparing the general behavior of plasticity rules during switches from wakefulness to sleep, we first parameterized all 20 model variations in the wakefulness state based on two well-established experi-

mental plasticity induction protocols (Figure 2B). In the first induction protocol, the time lag between pre- and postsynaptic spikes is tested for a given frequency after several pairs. This protocol permitted to experimentally uncover the STDP rule [27]. Figure 2C shows the average (black curve) and standard deviation (gray shadow) of the behavior of the different models after parameterization, together with the experimental data of [27] (circles). In the second induction protocol, a fixed time lag is maintained while the impact of the stimulation frequency is explored. Similarly, Figure 2D shows the average (black curve) and standard deviation (gray shadow) of the behavior of the different models after parameterization for the second protocol, together with the experimental data [28] (circles). More information on the protocols can be found in *SI Appendix*. For each model, a specific datasheet provides the parameter values as well as the validation on experimental data and the evolution of the synaptic weight during burst mode (see *SI Appendix*).

We generalized the computational experiment performed in Figure 1B to all 20 synaptic model variations (see *SI Appendix* for a simulation trace of each individual simulation). In all model configurations implementing a soft bound, a network switch from wakefulness mode to sleep mode generated a homeostatic reset of synaptic weights, very reminiscent of what is shown in 1B. In all model configurations implementing a hard bound, a network switches from wakefulness mode to sleep mode generated a convergence of the synaptic weights towards the extreme value with a constant velocity whatever its initial weight. Such saturation phenomenon of all synaptic weights was previously shown in other applications (see for instance [38]). Although the convergence dynamics are different between the two cases, the outcome is the same: a switch to sleep regularizes synaptic weights, potentially disrupting any learning that might have occurred during the wakefulness period. This shows that such sleep-induced homeostatic reset of synaptic weights is a robust phenomenon that does not depend on the specifics of any synaptic plasticity model.

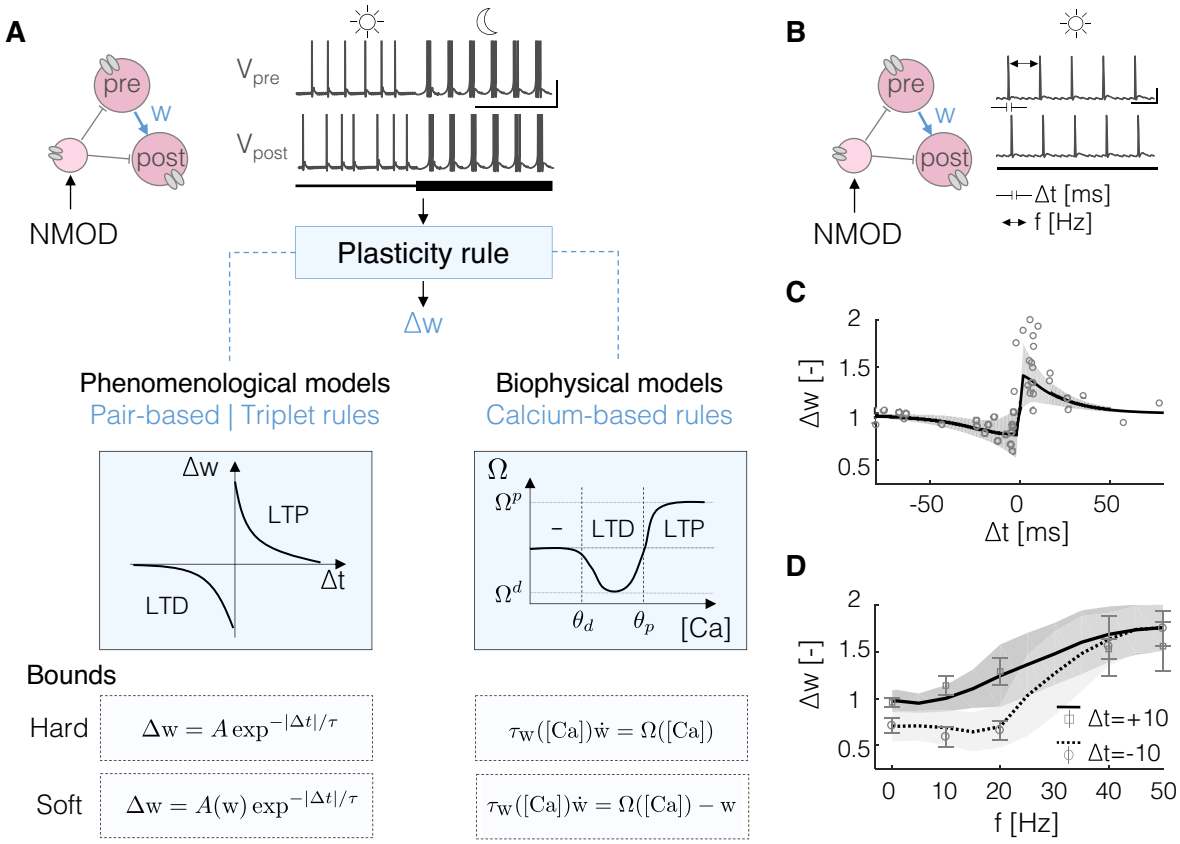

Figure 2: Two categories of synaptic plasticity rules reproduce experimental data from plasticity-induced protocol.
A. A three-cell circuit able to switch from tonic to burst. The synaptic weight w between pre- and postsynaptic neurons is affected by plasticity. Two categories of plasticity rules are tested. (Left) *Phenomenological models* focusing on the spike timing such as the pair-based and triplet models [14, 15, 25] such as $w \to w + \Delta w$ and $\Delta t = t_{\text{post}} - t_{\text{pre}}$. The weight-dependency is affecting the potentiation/depression parameter A. (Right) *Biophysical models* use the intracellular calcium to drive synaptic change such as $\tau_w([\text{Ca}])\dot{w} = F(w, [\text{Ca}])$. Small (resp. high) calcium level leads to slow (resp. fast) depression (resp. potentiation). Either the plasticity rule is a continuous function of calcium (as in [17]) or use depression and potentiation levels (Ω^{d} and Ω^{p}) associated to two calcium thresholds (depression or potentiation θ_{d} or θ_{p}), as in [25]). The weight-dependency modifies the synaptic plasticity equation.
B. Plasticity induced protocols focus on maintaining either the simulation frequency and varying the pre- and post-spike time $\Delta t = t_{\text{post}} - t_{\text{pre}}$ [27] or maintaining a constant time lag and varying the spike frequency f [28].
C. The change of synaptic strength (Δw) is shown as a function of the pre-post pairings (Δt) for a frequency of 1 Hz, reproducing [27] experimental data (circles). The fit obtained in all models for hippocampus data is averaged. The mean (black line) and the standard deviation (gray shadow) are shown.
D. The change of the synaptic strength is shown as a function of frequency pairings for regular pre-post pairs ($\Delta t = 10$ ms (full line) and $\Delta t = -10$ ms (dotted line)) reproducing [28] experimental data obtained in cortex (circles, squares, mean + std). The fit obtained in all models is averaged. The mean and standard deviation are shown by the black line and the gray shadow, respectively.

The homeostatic reset is robust to variability and heterogeneity in circuit parameters

We next tested the robustness of the homeostatic reset to changes in the parameters of the neuronal circuits. We introduced variability in three parameters: (i) the level of neuromodulator concentration, which is modeled by a variable inhibitory drive onto the circuit inhibitory neuron (Figure 3A), (ii) variability in neuron intrinsic parameters such as maximal conductance values (Figure 3B), and (iii) network size, with the introduction of heterogeneity in neuron parameters within the network (Figure 3C).

The results of a variability in neuromodulator concentration is shown in Figure 3A. At the circuit

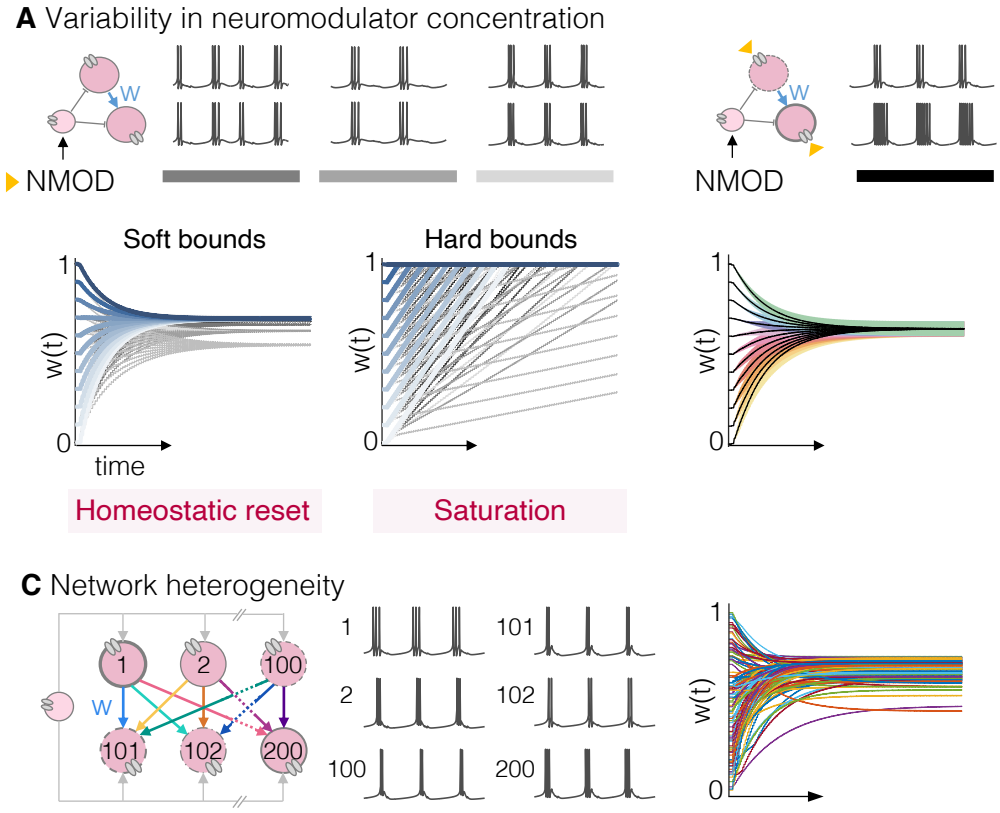

Figure 3: The homeostatic reset occurs for the different category of synaptic plasticity rules and is robust to intrinsic variability and network heterogeneity.
A. Pre- and postsynaptic neurons burst under neuromodulatory input. Different neuromodulator concentrations lead to different bursting patterns (gray line - top traces). The time evolution of the synaptic weight is computed in all synaptic plasticity models considering two weight-dependencies. (Left) Soft bounds lead to a *homeostatic reset* (each blue line is associated to one initial value). The value of the reset is altered by bursting patterns (see gray lines). (Right) For hard bounds, all synaptic weights saturate to the extreme values at different rates depending on the burst profile. (Time window: 40 s.)
B. 10 circuits are generated with variability in their intrinsic parameters affecting the bursting rhythm. Each circuit shows the homeostatic reset. (Averaged weight in black line and its standard deviation in color shadow, time duration: 40 s.).
C. A fully connected feedforward network of 100 pre to 100 postsynaptic neurons is built with heterogeneous intrinsic variability. All initial weights are initialized at random values between 0 and 1. Despite heterogeneity in the network, all synaptic weights present the homeostatic reset and converge towards the same range of values. Each voltage trace lasts 0.9 s - y-scale: 140 mV, 100 weight traces among the 10000 are shown for model Ca 1, during 50 s.

level, different concentrations of neuromodulator leads to diverse bursting patterns. These bursting patterns vary in terms of the number of spikes per burst, the intraburst frequency, the interburst frequency and the duty cycle [1, 29], which can potentially strongly affect the behavior of the plasticity rules. However, a homeostatic reset of synaptic weights is observed each time the circuit enters a rhythmic pattern, and this reset is robust to the specific properties of the pattern itself. A change in rhythmic pattern solely affects the convergence rate and reset value in the case of soft bounds, and the slope of the linear convergence rate in the case of hard bounds (see Figure 3A, bottom panels, where the different shades of gray represent one circuit simulated with one neuromodulator level). The results show that the homeostatic reset is a robust phenomenon relying on network rhythmic state, but whose reset value is tunable through neuromodulation level.

We then added some variability in order to grow closer to what is observed in biological systems [1, 39–42]. To this end, ten circuits varying in their parameter sets of maximal intrinsic conductances and applied currents were simulated. The maximal conductances varied within an interval of 10 %. Each

circuit is first verified to switch from tonic to bursting mode. Similarly to neuromodulation level, introducing variability affects the bursting pattern, but also breaks the pattern symmetry between the presynaptic and postsynaptic neurons: each neuron exhibits differences in its neuronal rhythm (Figure 3B, top). This breaking of symmetry does not affect the outcome. In all 10 circuits, whatever the initial weight acquired in tonic mode, the synaptic weights reset in rhythmic mode. The exact value of the reset is simply slightly different in different circuits, as shown in Figure 3B, bottom (the mean evolution of the weights in the 10 circuits is shown in black, whereas the colored shadows depict the standard deviation for each initial condition). The mean reset value is equal to 0.6347 and the standard deviation is equal to 0.0108 for the biophysical model 2. For phenomenological models, the standard deviation is higher due to the sensitivity of the exact spike time inside the intraburst (for the pair-based model: mean = 0.6002, std = 0.0714).

Finally, network size was increased to account for the impact of heterogeneity between neurons of the same network. We built a heterogeneous network composed of 2 layers of 100 excitatory neurons each fully connected in a feedforward configuration. Each neuron has different intrinsic properties. The inhibitory neuron drives the transition from tonic to burst thanks to the neuromodulatory input (see Figure 3C, left).The network is initialized with random connectivity, mimicking a situation after a learning period (a similar procedure is done in [20, 21]). The neurons show different burst rhythms with various intraburst frequencies and different number of spikes per burst (see Figure 3, center). The evolution of the synaptic weights are displayed in Figure 3C, right. Network heterogeneity induces heterogeneity in reset values within the network. This heterogeneity is related to the variability in pre- and postsynaptic burst properties, it is not dependent on the initial synaptic weight (Figure 3C, right).

Altogether, these different computational experiments convincingly show that the mechanisms underlying the homeostatic reset of synaptic weights are robust to synaptic model type, the fitted region, the presence of short-term depression, the neuromodulation level, the neuronal circuit variability and the network heterogeneity. In all cases, strong weights decrease and weak weights grow toward a reset value. This exact value is moderately influenced by rhythm properties, hence tunable by neuromodulator level. Turning soft-bound into hard bound simply drives all the weights toward saturation.

The endogenous nature of rhythmic bursting leads to homeostatic reset

In order to gain more insights into the mechanisms underlying the homeostatic reset, and particularly understand why this phenomenon specifically occurs during sleep-dependent rhythmic activity, we analyzed how phenomenological and biophysical plasticity models interact with circuit rhythmic activity. In particular, we took advantage of previous analytical work linking the time evolution and convergence of synaptic weights to either spike time statistics (for phenomenological models) or calcium dynamics (for biophysical models) [22, 43–46].

In phenomenological models, the time evolution of a synaptic weight and its convergence occurs on a time interval much larger than typical interspike intervals. Therefore, following the work of [37, 47], we can average the dynamics of the synaptic weight (see Methods equation (1)) over a time interval T and get

$$\dot{w} = -A^- w^\mu \int_{-\infty}^{0} e^{s/\tau^-} C(s;t)ds + A^+(1-w)^\mu \int_{0}^{\infty} e^{-s/\tau^+} C(s;t)ds,$$

where A^+ and A^- are the potentiation and depression parameters (see Methods), μ stands for the weight-dependency, $e^{-|s|/\tau^\pm}$ stands for the STDP kernel in potentiation or depression with τ^+ and τ^- being the time-constants given in the pair-based model, and $C(s;t)$ is the (temporally averaged) correlation function between the pre and post spike trains, respectively noted $S_{\text{pre}}(t) = \sum_k \delta(t - t_{\text{pre},k})$ and $S_{\text{post}}(t) = \sum_k \delta(t - t_{\text{post},k})$, that is,

$$C(s;t) = \frac{1}{T}\int_{t}^{t+T} S_{\text{pre}}(\tau) S_{\text{post}}(\tau + s)d\tau.$$

Assuming the stationarity of both spike trains, the correlation function is time-invariant, *i.e.*, $C(s;t) = C(s)$, and the time evolution of the synaptic weight can be computed as [47]:

$$\dot{w} = A^+(1-w)^\mu C^+ - A^- w^\mu C^-,$$

where $C^+ = \int_0^\infty e^{-s/\tau^+} C(s)ds$ and $C^- = \int_{-\infty}^0 e^{s/\tau^-} C(s)ds$.

A qualitative analysis of this equation permits to understand why synaptic weights converge towards a single steady-state for any stationary value of $C(s)$, considering soft-bound dependency *i.e.* $\mu = 1$. The term $A^+(1-w)C^+$ computes the weight increase due to all postsynaptic spikes following presynaptic spikes considering the associated time lag. The term $A^- w C^-$ computes the weight decrease due to all postsynaptic spikes preceding presynaptic spikes. When modeling soft bounds, both terms are weight-dependent, which deforms the plasticity kernel (Figure 4A). When the synaptic weight is weak, the term $A^+(1-w)C^+$ dominates, and potentiation overcomes depression (Figure 4A, left). When the synaptic weight is strong, the term $A^- w C^-$ dominates, and depression overcomes potentiation (Figure 4A, center). The drift eventually stabilizes at the synaptic weight value for which depression balances potentiation, *i.e.*, $A^+(1-w)C^+ = A^- w C^-$ (Figure 4A, right). This convergence value can be computed analytically by solving this balance equation, which leads to a convergence value that is bound-dependent. The reset value w_{HR} is obtained analytically by

$$w_{\text{HR}} = \frac{\frac{A^+C^+}{A^-C^-}}{1 + \frac{A^+C^+}{A^-C^-}}.$$

This equation states that the reset value depends on a ratio between the potentiation parameter weighted by the correlation between pre-post spikes and the depression parameter weighted by the correlation between post-pre spikes.

We applied this methodology to compare the convergence of the synaptic weights in wakefulness and sleep modes. To this end, we used the previously built heterogeneous network composed of 2 layers of 100 excitatory neurons fully connected in a feedforward configuration (Figure 4B). The network is initialized with random connectivities. In wakefulness mode, excitatory neurons receive external stimulation at random frequencies, ranging from 0.01 Hz up to 50 Hz, which mimics the effect of sensory inputs, among others (Figure 4B, top). In sleep mode, a neuromodulatory drive to the inhibitory cell switches the network to sleep mode (Figure 4B, bottom).

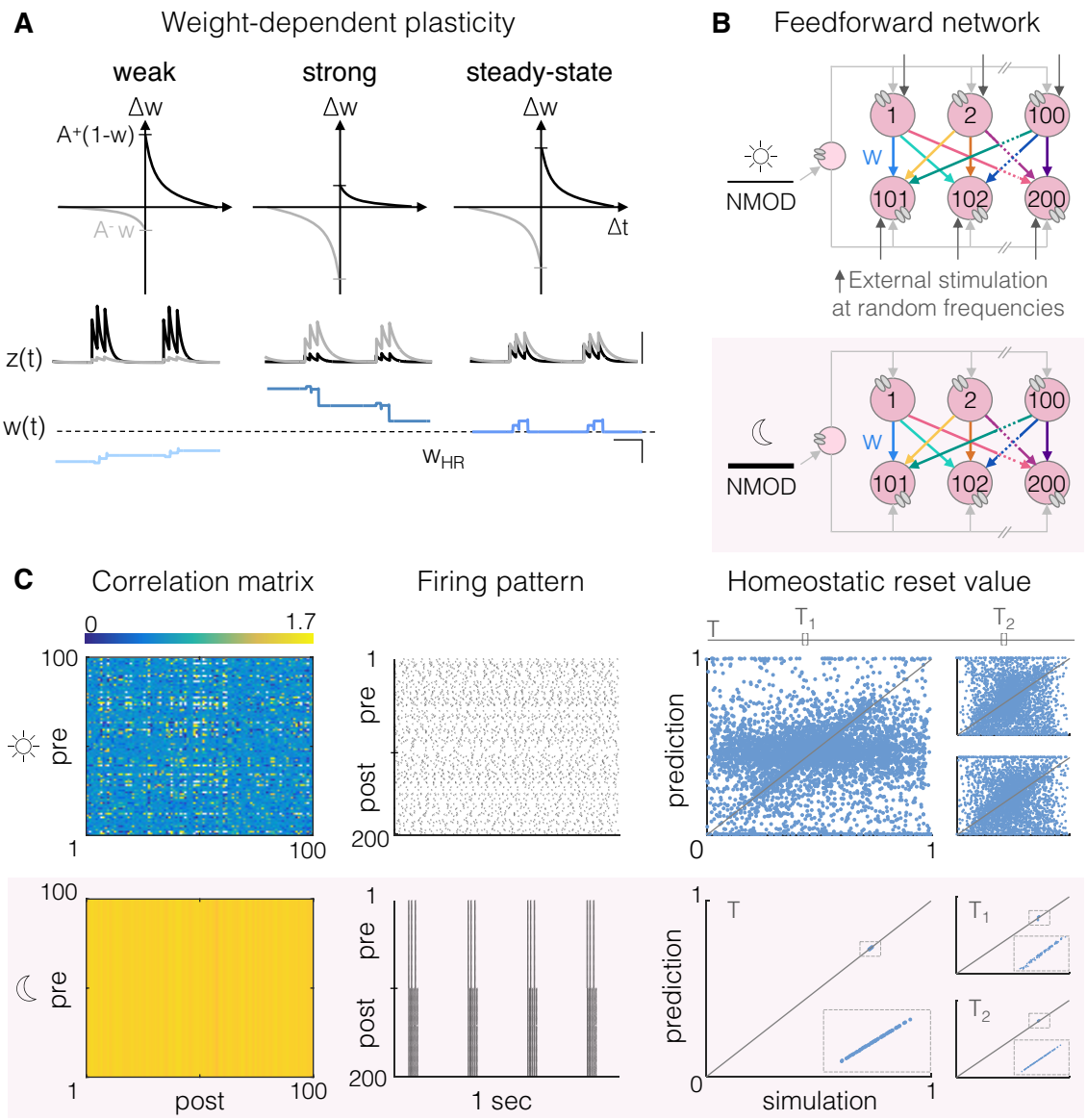

Figure 4: The homeostatic reset relies on the endogenous nature of rhythmic bursting during sleep.

A. Weight-dependent plasticity modulates the potentiation and depression parameters with respect to the synaptic weights. The spike-time dependent plasticity kernel is weight-dependent. The potentiation and depression traces are shown respectively in black and gray with the associated synaptic weight evolution considering two successions of endogenous burst (x-scale: 0.6 s, y-scale for z: 0.06 %, y-scale for w: 2.5 %.)

B. A 2-layer feedforward network with the same 100 neurons fully connected to the same 100 postsynaptic neurons. All the synaptic weights (resp. AMPA connections) are randomly initialized between 0 to 1 (resp. 0.01 to 4). In wakefulness, neurons are excited by external stimulation at random frequencies between 0.01 to 50 Hz. In sleep, the neuromodulation (NMOD) level drives the neurons in burst mode.

C. (Left) The correlation between presynaptic spike trains and postsynaptic spike trains are computed. We show the ratio between the positive correlation (C^+ associates to the potentiation correlation when a postsynaptic neuron spikes after a presynaptic neuron) and the negative correlation (C^- for a pre spikes after a post spikes) in spiking regime and sleep-like regime (resp. top and bottom). (Center, top) In wakefulness, neurons are in exogenous spiking mode. (Center, bottom) In sleep, neurons are in endogenous burst mode. (Right) The spike trains correlation is computed for the entire simulation T and compared with the correlation at two given times T_1 and T_2 (equal to 10 s and 40 s). Scatter plots between the reset value obtained via simulation (converging point) and the predicted value obtained analytically.

First, we computed the correlation ratio C^+/C^- between the pre and post (binary) spike trains for all 10 000 synaptically coupled pairs, both in wakefulness and sleep modes. The results are reported in

a correlation matrix for each mode (Figure 4C, left). These correlation matrices show that correlation values are highly heterogeneous in wakefulness mode, whereas they are highly homogeneous in sleep mode. This is due to the fact that spike trains are variable in wakefulness, whereas the network switches to a global, rhythmic activity in sleep mode (Figure 4C, center). As a consequence, synaptic weights are predicted to converge towards many different values in wakefulness, but towards very similar values in sleep, which partially explains why the homeostatic reset is only observed during sleep.

Secondly, we compared the synaptic weight values obtained from model simulations with the prediction values w_{HR}. Prediction values were computed on the complete time period T, as well as on two transient time periods T_1 and T_2, and results are provided on a raster plot for each time period in both modes (Figure 4C, right - mean prediction error +- standard deviation over 8 different neuromodulator drives: mean = 0.0031, std= 0.0027, see *SI Appendix* for details). The figures show that, although there is an almost perfect match between simulated and predicted reset values in sleep mode, simulated synaptic weights do not converge towards their predicted values during wakefulness for any time window. This is explained by the assumption that the correlation function between the spike trains is stationary over the time windows, *i.e.*, $C(s;t) \approx C(s)$, is only true in sleep mode, due to the endogenous nature of the rhythmic bursting activity. As a result, a reset of synaptic weights is only really observed during sleep.

In biophysical models, a similar analytical approach can be derived based on calcium dynamics by comparing the time spent in depression and potentiation [18]. Again the time evolution of a synaptic weight and its convergence occur on a time interval much larger than typical calcium oscillations. Therefore, we can average the dynamics of the synaptic weight (see Methods equation (2)) over a time interval T and get

$$\dot{w} = \frac{1}{T}\int_t^{t+T} \frac{1}{\tau_w([\mathrm{Ca}](\tau))}\left[\Omega([\mathrm{Ca}](\tau)) - \mu\, w\right] d\tau,$$

where $\Omega([\mathrm{Ca}])$ and $\tau_w([\mathrm{Ca}])$ are functions that map intracellular calcium concentration to potentiation (Ω^{p}) and depression (Ω^{d}) levels and potentiation (τ^{p}) and depression (τ^{d}) time-constants, as in [25] (see *SI Appendix*). We note the effective time spent in each region α^{d} and α^{p} as the time spent balanced by the time-constant of potentiation/depression in the corresponding region, that is,

$$\alpha^{\mathrm{d}} = \frac{1}{\tau_{\mathrm{d}}}\frac{1}{T}\int_t^{t+T} I(\theta_{\mathrm{d}} < [\mathrm{Ca}](\tau) < \theta_{\mathrm{p}}) d\tau,$$
$$\alpha^{\mathrm{p}} = \frac{1}{\tau_{\mathrm{p}}}\frac{1}{T}\int_t^{t+T} I([\mathrm{Ca}](\tau) > \theta_{\mathrm{p}}) d\tau,$$

where $I(x)$ is the indicator function equals 1 when x is true and 0 when x is false. The synaptic weights reach a stable state once the potentiation level Ω^{p} and the depression level Ω^{d} weighted by their effective time spent in the corresponding regions are balanced. It gives

$$w_{\mathrm{HR}} = \frac{\Omega^{\mathrm{d}}\alpha^{\mathrm{d}} + \Omega^{\mathrm{p}}\alpha^{\mathrm{p}}}{\alpha^{\mathrm{d}} + \alpha^{\mathrm{p}}}.$$

The comparison between the value of the homeostatic reset obtained via computational simulations and the analytic approach is provided in *SI Appendix, Tab.S7*. Again, w_{HR} is only predictive if the effective time spent in each region α^{d} and α^{p} can be considered stable over time, which is only true in sleep mode, as attested by the good match between predicted and simulated reset values (mean prediction error+-standard deviation over 8 different neuromodulatory drives: mean error = 0.0016, std= 0.0019)).

Finally, both analytical analyses can be extended to the case of hard bounds. In this case, all synaptic weights converge towards saturation in sleep mode, and the saturation speed λ, or slope, depends on the neuromodulatory drive. In phenomenological models, this saturation slope can be predicted by the equation

$$\lambda = A^+C^+ - A^-C^-,$$

where T is the time-window considered to compute the correlation. In biophysical models, the saturation slope corresponds to the sum of the depression rate and potentiation rate, each weighted by the fraction of time spent in their corresponding regions α^{d} and α^{p}, which writes

$$\lambda = \alpha^{\mathrm{p}}\Omega^{\mathrm{p}} + \alpha^{\mathrm{d}}\Omega^{\mathrm{d}}.$$

The values of the saturation slope obtained via computational simulations match the analytic predictions for both model types (*SI Appendix, Tab.S7* - calcium model: mean error = 0.049, std= 0.039, pair-based model: mean error = 0.027, std= 0.033 over 8 neuromodulatory drives). Complementary explanations about the origin of the homeostatic reset are available in *SI Appendix.*

In summary, analytical analyses of the mechanisms underlying time evolution of synaptic weights showed that a homeostatic reset solely occurs during sleep mode due to the endogenous, global nature of the network rhythmic activity in this mode, both in phenomenological models and biophysical models of synaptic plasticity.

Discussion

A key step in understanding how switches in brain states affect memory encoding is finding ways to study the interactions between synaptic plasticity rules and neuromodulation of brain activity. It represents a challenge, as plasticity rules and neuromodulation target neurons at the molecular and cellular levels, whereas brain states and memory emerge at the population level. In this work, we leverage the power of computational modeling to study how network connections formed via any of 20 variations of 7 well-established plasticity rules are affected by a switch from asynchronous tonic spiking to rhythmic bursting, mimicking wakefulness to sleep transitions. We showed that transitions from wakefulness to sleep induce a homeostatic reset of all synaptic weights towards a specific value for all tested synaptic plasticity rules.

For a newly described phenomenon in a computational modeling work to be of physiological relevance, it has to be shown that it does not arise from an artifact of the choice of models and parameters used in the study. We therefore thoroughly tested the robustness of the homeostatic reset to variability in models and parameters. First, we showed that the homeostatic reset arises from both phenomenological models and biophysical models of synaptic plasticity, which ruled out the possibility of an artifact of the chosen model type. Second, the homeostatic reset was shown to be robust to changes in neuromodulator drive, variability in neuron and circuit parameters, and heterogeneity in larger neuronal populations. Changes in neuromodulator drive however affected the reset value, which suggests that the homeostatic reset is both a robust and tunable phenomenon. Finally, using mathematical analyses that directly link firing activity or calcium dynamics to changes in synaptic weights, we showed that the homeostatic reset is limited to the sleep period due to the highly endogenous, rhythmic activity globally shared by the network during that period.

The main effect of the homeostatic reset is that it regularizes synaptic weights during sleep, or more specifically synaptic efficacy, regardless of their evolution during the previous day. The consequences of this regularization are twofold. On the one hand, it provides a mechanism by which synaptic efficacy returns to a homeostatic set-point during sleep, restoring the ability of the network to learn new information on the next day. Such a mechanism could play a central role in sleep homeostasis [48–50]. On the other hand, the homeostatic reset disrupts any learning that occurred during the previous day, which could lead to catastrophic forgetting [51]. This forgetting may be overcome via mechanisms that transfer learning encoded in synaptic efficacy into long-lasting, structural changes in synaptic connections, such as the number of receptors at each synapse, the number and size of synapses, etc [52, 53]. Another possibility would be to overcome the homeostatic reset itself through sleep-induced changes in synaptic rules, which could be controlled by neuromodulators [20, 54–56].

The results presented in this work put forward new challenges in experimental and computational study of synaptic plasticity and memory formation. We showed that maintaining learning rules extracted from stereotyped plasticity protocol obtained in spiking mode is incompatible with sleep-dependent memory consolidation. New plasticity-induction protocols, which consider the endogenous bursting rhythm rather than imposing in-vitro spiking regime for instance, would provide a novel viewpoint on synaptic plasticity rules [57]. Adding neuromodulators to drive the switches in activity and potentially plasticity rules during the experiments could also provide novel insights. From a computational viewpoint, this work highlights the importance of using models of neurons and networks that are capable of switching between different physiologically relevant firing activities. It suggests going beyond using spike-times or the output of reduced models such as integrate-and-fire neuron models as input to the synaptic plasticity rule when studying sleep-dependent memory consolidation.

Methods

Simulations were performed using the Julia programming language [58]. Analyses were performed either in Matlab or Excel. Code files are freely available at `https://github.com/KJacquerie/HomeostaticReset`.

Conductance-based modeling

All neurons are modeled using a single-compartment Hodgkin and Huxley formalism. The membrane voltage V_m evolves as follows [1, 29]:

$$C_{\mathrm{m}}\dot{V}_{\mathrm{m}} = -\sum_i I_{\mathrm{ion},i} + I_{\mathrm{app}}$$

where C_{m} is the membrane capacitance, $I_{\mathrm{ion},i}$ is the ith current carried by ionic channels i, and I_{app} is an external applied current. The description of the ionic currents and the associated parameters are described in *SI Appendix*.

The neuron circuit is composed of three neurons. An inhibitory neuron (I) is connected to two excitatory neurons through $\mathrm{GABA_A}$ and $\mathrm{GABA_B}$ connections. The two excitatory neurons are connected in one direction through an AMPA synapse, the afferent neuron is called the presynaptic (pre) neuron, and the efferent neuron is called the postsynaptic (post) neuron. The synaptic currents are described in *SI Appendix*.

The inhibitory cell controls the rhythm of the circuit. A tonic rhythm in the inhibitory neuron puts the two excitatory cells in a resting state. If the pre- or the postsynaptic cell receives a depolarizing pulse, they generate an action potential. An hyperpolarizing current applied to the inhibitory neuron switches the whole circuit in rhythmic bursting mode. This hyperpolarizing current model the effect of a neuromodulator signal (NMOD) [8].

Synaptic plasticity

The synaptic connection between the presynaptic neuron and the postsynaptic neuron is subjected to plasticity. The time evolution of this connection is studied during both tonic and bursting modes. This AMPA synapse is modeled by $g_{\mathrm{AMPA}} = w\bar{g}_{\mathrm{AMPA}}$ where w the synaptic weight, and $\bar{g}_{\mathrm{AMPA}}$ isthe constant maximal conductance. A very small initial connectivity $\bar{g}_{\mathrm{AMPA}}$ equal to $0.01\,\mathrm{mS/cm^2}$ is taken such as the induced Excitatory Post-Synaptic Potential (EPSP) at the postsynaptic site does not initiate a spike. The variable w is weighing the synaptic current and is driven by a synaptic plasticity rule.

Two main categories of synaptic plasticity rules are explored in this paper: phenomenological rules and calcium-based rules. The first category uses the pre- and postsynaptic spike times to drive the synaptic change while the second category uses the calcium signal.

Phenomenological models

The pair-based model considers the pre- and postsynaptic spike time (resp. t_{pre} and t_{post}) with a time difference $\Delta t = t_{\mathrm{post}} - t_{\mathrm{pre}}$ to induce the change in synaptic weight. To reproduce the classical STDP window, a pair-based model was implemented [14, 16, 22–24]:

$$w \to \begin{cases} w + A^+(1-w)^\mu e^{-\Delta t/\tau^+}, & \text{at } t_{\mathrm{post}} \text{ if } t_{\mathrm{pre}} < t_{\mathrm{post}}, \\ w - A^- w^\mu e^{\Delta t/\tau^-}, & \text{at } t_{\mathrm{pre}} \text{ if } t_{\mathrm{pre}} > t_{\mathrm{post}}, \end{cases}$$

where $A^+ > 0$, $A^- > 0$ and μ is the weight-dependency parameter (μ is equal to 1 for soft-bounds and to 0 for hard-bounds) [16, 24]. The functions $e^{-|\Delta t|/\tau^\pm}$ are the temporal kernel of potentiation and depression. If we introduce $S_{\mathrm{pre}}(t) = \sum_k \delta(t - t_{\mathrm{pre},k})$ and $S_{\mathrm{post}}(t) = \sum_k \delta(t - t_{\mathrm{post},k})$ for the spike trains of pre- and postsynaptic neurons, the evolution of the synaptic weight can be written as follows:

$$\dot{w} = -A^- w^\mu \left[\int_{-\infty}^{0} e^{s/\tau^-} S_{\mathrm{post}}(t-s)ds\right] S_{\mathrm{pre}}(t) + A^+(1-w)^\mu \left[\int_0^{\infty} e^{-s/\tau^+} S_{\mathrm{pre}}(t-s)ds\right] S_{\mathrm{post}}(t). \quad (1)$$

The triplet-based model extends the pair-based model to account for three spikes patterns, such as pre-post-pre and post-pre-post [15]. Similarly to pair-based model, the triplet model was implemented using trace variables following [15]. More details are provided in *SI Appendix*.

Biophysical models

Calcium dynamics are modeled following [18, 25]. The global equation for calcium-dependent plasticity rule can be written such as

$$\tau_w([\mathrm{Ca}])\dot{w} = \Omega([\mathrm{Ca}]) - \mu\, w, \tag{2}$$

where μ modulates the weight-dependency: $\mu = 0$ (resp. $\mu = 1$) refers to hard (resp. soft) bounds. In total, five major calcium-based dependent models are investigated in this paper. Some rules were adapted to fit either *frequency-dependent protocol* (cortical experimental data) or a *STDP* protocol (hippocampus experimental data). Different *weight-dependencies* (soft bounds or hard bounds) are compared. The impact of the *coupling* between the presynaptic calcium influx and the synaptic weight or the presence of *short-term depression* are also tested [26]. Calcium-based rules are either implemented using two-triggered calcium thresholds for potentiation and depression, or using a continuous function for the calcium dependency. More details are provided in *SI Appendix*.

Computational experiments

Figure 1B simulates two successive periods of tonic activity (wakefulness) and bursting activity (sleep) of 40 s each for 6 neuronal circuits. During wakefulness, correlated circuits are obtained by applying pre-post pairs of spikes at different frequencies that induces an increase in synaptic weight. For uncorrelated circuits, pre and post cells fire independently at the nominal same frequency f_0. Spike timings are generated with interspike intervals following independent Normal distributions $\mathcal{N}(\frac{1}{f_0}, (\frac{0.3}{f_0})^2)$. During sleep, the level of neuromodulators is modeled by an hyperpolarizing current applied to the inhibitory neuron (more details in *SI Appendix*).

In Figure 3A, the variability in neuromodulator concentrations (shades of gray) is obtained by applying different applied current to the inhibitory cell, ranging from -1 to $-1.7\,\mathrm{nA/cm^2}$ resulting in different bursting patterns (see all traces in *SI Appendix, Fig.S5*). Figure 3B depicts the mean of the synaptic weight time evolution for 10 circuits in which variability in the ionic conductances is added. Each circuit is initialized with maximal conductances that are randomly picked with respect to an uniform distribution in an interval of 10 % around its nominal value $\bar{g}_0$, such as $[\bar{g}_0 - 0.1\bar{g}_0, \bar{g}_0 + 0.1\bar{g}_0]$. The plasticity rule used is the calcium model from [25]. Figure 3C considers a network of 2 layers with 100 presynaptic neurons fully connected to 100 postsynaptic neurons in a feedforward configuration. The connections (colors) are initialized randomly between 0 and 1. Intrinsic parameters of all cells are randomized by adding variability in the ionic conductances $g_{\mathrm{K,Ca}}$ and $g_{\mathrm{Ca,T}}$ in the same way as in the Figure 3B, with 20 % variability. The plasticity rule used is the calcium model from [25].

Synaptic weight equilibrium value can be found by analytical demonstration (see on *SI Appendix* for details).

Figure 4A shows the kernel of spike-time dependent plasticity considering the synaptic weight-dependency. It unravels the effective value of the potentiation and depression increment respectively labeled $A^+(1-w)$ and A^-w. Figure 4C (left) gives the ratio between the positive and negative correlation. The positive correlation describes the correlation for presynaptic spike followed by a postsynaptic spike. The negative correlation describes the inverse relation for a postsynaptic spike followed by a presynaptic spike. Figure 4C (right), the simulated value is equal to the converging value in the time evolution of the synaptic weight. The predicted value is computed from the analytical formula provided w_{HR}.

More details on all computational experiments can be found on *SI Appendix*.

Acknowledgments

This work was supported by the Belgian National Fund for Scientific Research - FNRS (ID application: 34959817).

References

[1] Kathleen Jacquerie and Guillaume Drion. "Robust switches in thalamic network activity require a timescale separation between sodium and T-type calcium channel activations". In: *PLOS Computational Biology* 17.5 (2021), e1008997. DOI: 10.1371/journal.pcbi.1008997.

[2] György Buzsáki. "Memory consolidation during sleep: a neurophysiological perspective". In: *Journal of Sleep Research* 7.S1 (1998), pp. 17–23. DOI: 10.1046/j.1365-2869.7.s1.3.x.

[3] Joseph Chrol-Cannon and Yaochu Jin. "Computational modeling of neural plasticity for self-organization of neural networks". In: *Biosystems* 125 (2014), pp. 43–54. DOI: 10.1016/j.biosystems.2014.04.003.

[4] Andrea A. Kühn et al. "Event-related beta desynchronization in human subthalamic nucleus correlates with motor performance". In: *Brain* 127.4 (2004), pp. 735–746. DOI: 10.1093/brain/awh106.

[5] David A. McCormick and David B. Salkoff. "Brain State Dependent Activity in the Cortex and Thalamus". In: *Current Opinion in Neurobiology* 31 (2015), pp. 133–140. DOI: 10.1016/j.conb.2014.10.003.

[6] S M Sherman. "Tonic and burst firing: dual modes of thalamocortical relay." In: *Trends in neurosciences* 24.2 (2001), pp. 122–6. DOI: 10.1016/S0166-2236(00)01714-8.

[7] Eve Marder, Timothy O'Leary, and Sonal Shruti. "Neuromodulation of Circuits with Variable Parameters: Single Neurons and Small Circuits Reveal Principles of State-Dependent and Robust Neuromodulation". In: *Annual Review of Neuroscience* 37.1 (2014), pp. 329–346. DOI: 10.1146/annurev-neuro-071013-013958.

[8] Edward Zagha and David A. McCormick. "Neural control of brain state". In: *Current Opinion in Neurobiology* 29.1 (2014). Publisher: Elsevier Ltd, pp. 178–186. DOI: 10.1016/j.conb.2014.09.010.

[9] P. Maquet. "The role of sleep in learning and memory". In: *Science* 294.5544 (2001), pp. 1048–1052. DOI: 10.1126/science.1062856.

[10] Matthew P. Walker and Robert Stickgold. "Sleep-Dependent Learning and Memory Consolidation". In: *Neuron* 44.1 (Sept. 2004). Publisher: Cell Press, pp. 121–133. DOI: 10.1016/J.NEURON.2004.08.031.

[11] Robert Stickgold. "Sleep-dependent memory consolidation". In: *Nature* 437.7063 (2005), pp. 1272–1278. DOI: 10.1038/nature04286.

[12] Ami Citri and Robert C. Malenka. "Synaptic plasticity: Multiple forms, functions, and mechanisms". In: *Neuropsychopharmacology* 33.1 (2008), pp. 18–41. DOI: 10.1038/sj.npp.1301559.

[13] Ruth Heidelberger et al. "Synaptic Plasticity". In: *From Molecules to Networks: An Introduction to Cellular and Molecular Neuroscience: Third Edition*. Elsevier Inc., 2014, pp. 533–561. DOI: 10.1016/B978-0-12-397179-1.00018-X.

[14] L. F. Abbott and Sacha B. Nelson. "Synaptic plasticity: Taming the beast". In: *Nature Neuroscience* 3.11 (2000), pp. 1178–1183. DOI: 10.1038/81453.

[15] Jean Pascal Pfister and Wulfram Gerstner. "Triplets of spikes in a model of spike timing-dependent plasticity". In: *Journal of Neuroscience* 26.38 (2006), pp. 9673–9682. DOI: 10.1523/JNEUROSCI.1425-06.2006.

[16] Sen Song, Kenneth D. Miller, and L. F. Abbott. "Competitive Hebbian learning through spike-timing-dependent synaptic plasticity". In: *Nature Neuroscience* 3.9 (2000), pp. 919–926. DOI: 10.1038/78829.

[17] Harel Z. Shouval, Mark F. Bear, and Leon N. Cooper. "A unified model of NMDA receptor-dependent bidirectional synaptic plasticity". In: *Proceedings of the National Academy of Sciences of the United States of America* 99.16 (2002), pp. 10831–10836. DOI: 10.1073/pnas.152343099.

[18] Michael Graupner and Nicolas Brunel. "Calcium-based plasticity model explains sensitivity of synaptic changes to spike pattern, rate, and dendritic location". In: *Proceedings of the National Academy of Sciences of the United States of America* 109.10 (2012), pp. 3991–3996. DOI: 10.1073/pnas.1109359109.

[19] Umberto Olcese, Steve K. Esser, and Giulio Tononi. "Sleep and synaptic renormalization: A computational study". In: *Journal of Neurophysiology* 104.6 (2010), pp. 3476–3493. DOI: 10.1152/jn.00593.2010.

[20] Ana González-Rueda et al. "Activity-Dependent Downscaling of Subthreshold Synaptic Inputs during Slow-Wave-Sleep-like Activity In Vivo". In: *Neuron* 97.6 (2018), 1244–1252.e5. DOI: 10.1016/j.neuron.2018.01.047.

[21] Michael Jan Fauth and Mark C.W. Van Rossum. "Self-organized reactivation maintains and reinforces memories despite synaptic turnover". In: *eLife* 8.2018 (2019), pp. 1–19. DOI: 10.7554/eLife.43717.

[22] Jonathan Rubin, Daniel D. Lee, and H. Sompolinsky. "Equilibrium Properties of Temporally Asymmetric Hebbian Plasticity". In: *Physical Review Letters* 86.2 (2001), pp. 364–367. DOI: 10.1103/PhysRevLett.86.364.

[23] Mark C.W. Van Rossum, G. Q. Bi, and Gina G. Turrigiano. "Stable Hebbian learning from spike timing-dependent plasticity". In: *Journal of Neuroscience* 20.23 (2000), pp. 8812–8821. DOI: 10.1523/jneurosci.20-23-08812.2000.

[24] Abigail Morrison, Markus Diesmann, and Wulfram Gerstner. "Phenomenological models of synaptic plasticity based on spike timing". In: *Biological Cybernetics* 98.6 (2008), pp. 459–478. DOI: 10.1007/s00422-008-0233-1.

[25] Michael Graupner, Pascal Wallisch, and Srdjan Ostojic. "Natural firing patterns imply low sensitivity of synaptic plasticity to spike timing compared with firing rate". In: *Journal of Neuroscience* 36.44 (2016), pp. 11238–11258. DOI: 10.1523/JNEUROSCI.0104-16.2016.

[26] Nicolas Deperrois and Michael Graupner. "Short-term depression and long-term plasticity together tune sensitive range of synaptic plasticity". In: *PLoS Computational Biology* 16.9 (2020), pp. 1–25. DOI: 10.1371/journal.pcbi.1008265.

[27] Guo Qiang Bi and Mu Ming Poo. "Synaptic modifications in cultured hippocampal neurons: Dependence on spike timing, synaptic strength, and postsynaptic cell type". In: *Journal of Neuroscience* 18.24 (1998), pp. 10464–10472. DOI: 10.1523/jneurosci.18-24-10464.1998.

[28] Per Jesper Sjöström, Gina G Turrigiano, and Sacha B Nelson. "Rate, Timing, and Cooperativity Jointly Determine Cortical Synaptic Plasticity". In: *Neuron* 32.6 (2001), pp. 1149–1164. DOI: https://doi.org/10.1016/S0896-6273(01)00542-6.

[29] Guillaume Drion et al. "Switchable slow cellular conductances determine robustness and tunability of network states". In: *PLoS Computational Biology* 14.4 (2018), pp. 1–20. DOI: 10.1371/journal.pcbi.1006125.

[30] David A. McCormick and Thierry Bal. "Sleep and arousal: Thalamocortical mechanisms". In: *Annual Review of Neuroscience* 20 (1997), pp. 185–215. DOI: 10.1146/annurev.neuro.20.1.185.

[31] Mircea Steriade, Igor Timofeev, and François Grenier. "Natural waking and sleep states: A view from inside neocortical neurons". In: *Journal of Neurophysiology* 85.5 (2001), pp. 1969–1985. DOI: 10.1152/jn.2001.85.5.1969.

[32] S. Murray Sherman and R. W. Guillery. "Functional organization of thalamocortical relays". In: *Journal of Neurophysiology* 76.3 (1996), pp. 1367–1395. DOI: 10.1152/jn.1996.76.3.1367.

[33] Maxim Bazhenov et al. "Model of thalamocortical slow-wave sleep oscillations and transitions to activated states". In: *Journal of Neuroscience* 22.19 (2002), pp. 8691–8704. DOI: 10.1523/jneurosci.22-19-08691.2002.

[34] Sean Hill and Giulio Tononi. "Modeling sleep and wakefulness in the thalamocortical system". In: *Journal of Neurophysiology* 93.3 (2005), pp. 1671–1698. DOI: 10.1152/jn.00915.2004.

[35] Mark Humphries. "Dopaminergic control of the exploration-exploitation trade-off via the basal ganglia". In: *Frontiers in Neuroscience* 6 (2012). DOI: 10.3389/fnins.2012.00009.

[36] Mark C. W. van Rossum, Maria Shippi, and Adam B. Barrett. "Soft-bound Synaptic Plasticity Increases Storage Capacity". In: *PLoS Computational Biology* 8.12 (2012). Ed. by Peter E. Latham, e1002836. DOI: 10.1371/journal.pcbi.1002836.

[37] R. Gütig et al. "Learning Input Correlations through Nonlinear Temporally Asymmetric Hebbian Plasticity". In: *The Journal of Neuroscience* 23.9 (May 2003), pp. 3697–3714. DOI: 10.1523/JNEUROSCI.23-09-03697.2003.

[38] Jen Yung Chen et al. "Heterosynaptic plasticity prevents runaway synaptic dynamics". In: *Journal of Neuroscience* 33.40 (2013), pp. 15915–15929. DOI: 10.1523/JNEUROSCI.5088-12.2013.

[39] Eve Marder and Adam L. Taylor. "Multiple models to capture the variability in biological neurons and networks". In: *Nature Neuroscience* 14.2 (2011). Publisher: Nature Publishing Group, pp. 133–138. DOI: 10.1038/nn.2735.

[40] Julijana Gjorgjieva, Guillaume Drion, and Eve Marder. "Computational implications of biophysical diversity and multiple timescales in neurons and synapses for circuit performance". In: *Current Opinion in Neurobiology* 37.Table 1 (2016). Publisher: Elsevier Ltd, pp. 44–52. DOI: 10.1016/j.conb.2015.12.008.

[41] David J. Schulz, Jean Marc Goaillard, and Eve Marder. "Variable channel expression in identified single and electrically coupled neurons in different animals". In: *Nature Neuroscience* 9.3 (2006), pp. 356–362. DOI: 10.1038/nn1639.

[42] Eve Marder et al. "Memory from the dynamics of intrinsic membrane currents". In: *Proceedings of the National Academy of Sciences of the United States of America* 93.24 (1996), pp. 13481–13486. DOI: 10.1073/pnas.93.24.13481.

[43] Guy Billings and Mark C. W. van Rossum. "Memory Retention and Spike-Timing-Dependent Plasticity". In: *Journal of Neurophysiology* 101.6 (2009), pp. 2775–2788. DOI: 10.1152/jn.91007.2008.

[44] Joanna Jędrzejewska-Szmek et al. "Calcium dynamics predict direction of synaptic plasticity in striatal spiny projection neurons". In: *European Journal of Neuroscience* 45.8 (Apr. 2017). Ed. by Panayiota Poirazi, pp. 1044–1056. DOI: 10.1111/ejn.13287.

[45] Baktash Babadi and L. F. Abbott. "Stability and Competition in Multi-spike Models of Spike-Timing Dependent Plasticity". In: *PLoS Computational Biology* 12.3 (2016). DOI: 10.1371/journal.pcbi.1004750.

[46] Youngjin Park, Woochul Choi, and Se-Bum Paik. "Symmetry of learning rate in synaptic plasticity modulates formation of flexible and stable memories". In: *Scientific Reports* 7.1 (Dec. 2017), p. 5671. DOI: 10.1038/s41598-017-05929-2.

[47] Robert A Legenstein and Wolfgang Maass. "A Criterion for the Convergence of Learning with Spike Timing Dependent Plasticity." In: *Advances in Neural Information Processing Systems*. 2005, p. 8.

[48] Chiara Cirelli. "Sleep, synaptic homeostasis and neuronal firing rates". In: *Current Opinion in Neurobiology* 44 (2017). Publisher: Elsevier Ltd, pp. 72–79. DOI: 10.1016/j.conb.2017.03.016.

[49] Igor Timofeev and Sylvain Chauvette. "Sleep-Wake and Cortical Synaptic Plasticity". In: *Handbook of Behavioral Neuroscience* 30 (2019). Publisher: Elsevier B.V., pp. 443–454. DOI: 10.1016/B978-0-12-813743-7.00029-3.

[50] Brendon O. Watson et al. "Network Homeostasis and State Dynamics of Neocortical Sleep". In: *Neuron* 90.4 (2016), pp. 839–852. DOI: 10.1016/j.neuron.2016.03.036.

[51] Oscar C González et al. "Can sleep protect memories from catastrophic forgetting?" In: *eLife* 9 (2020). DOI: 10.7554/elife.51005.

[52] Friedemann Zenke and Wulfram Gerstner. "Hebbian plasticity requires compensatory processes on multiple timescales". In: *Philosophical Transactions of the Royal Society B: Biological Sciences* 372.1715 (2017). DOI: 10.1098/rstb.2016.0259.

[53] Jannik Luboeinski and Christian Tetzlaff. "Memory consolidation and improvement by synaptic tagging and capture in recurrent neural networks". In: *Communications Biology* 4.1 (Dec. 2021), p. 275. DOI: 10.1038/s42003-021-01778-y.

[54] Victor Pedrosa and Claudia Clopath. "The role of neuromodulators in cortical plasticity. A computational perspective". In: *Frontiers in Synaptic Neuroscience* 8.JAN (2017), pp. 38–38. DOI: 10.3389/fnsyn.2016.00038.

[55] Alexandre Foncelle et al. "Modulation of spike-timing dependent plasticity: Towards the inclusion of a third factor in computational models". In: *Frontiers in Computational Neuroscience* 12.July (2018), pp. 1–21. DOI: 10.3389/fncom.2018.00049.

[56] Zuzanna Brzosko et al. "Sequential neuromodulation of Hebbian plasticity offers mechanism for effective reward-based navigation". In: *eLife* 6 (2017), e27756. DOI: 10.7554/eLife.27756.

[57] B. Birtoli. "Firing Mode-Dependent Synaptic Plasticity in Rat Neocortical Pyramidal Neurons". In: *Journal of Neuroscience* 24.21 (May 2004), pp. 4935–4940. DOI: 10.1523/JNEUROSCI.0795-04.2004.

[58] Jeff Bezanson et al. "Julia: A Fresh Approach to Numerical Computing". In: *SIAM Review* 59.1 (2017), pp. 65–98. DOI: 10.1137/141000671.